(Received 22 September 2024, Accepted 16 October 2024, Scheduled 27 October 2024)

Designing Fabric-Based Broadband Metamaterial Absorbers for Radar Operating Frequency Bands

Baojun Chen[1], Hao Yuan[2], Yanjie Ju[1,*], Yanbing Xue[1], Tianyu Jiao[2], Qinghua Liu[2], and Mengqiu Qian[2]

[1]*School of Electrical Engineering, Dalian Jiaotong University, Dalian 116028, Liaoning, China*
[2]*School of Railway Intelligent Engineering Engineering Dalian Jiaotong University, Dalian 116028, Liaoning, China*

ABSTRACT: With the increasing use of radar technology across various fields, electromagnetic pollution has become a growing concern, posing significant risks to human health. Consequently, there is a rising interest in developing wearable, flexible fabric-based absorbers that can efficiently absorb electromagnetic waves. However, the low dielectric constant of fabrics makes it challenging to achieve high absorption rates and broad bandwidth at low frequencies. To address this issue, in this study, we introduce a fabric-based broadband metamaterial absorber using felt as the dielectric substrate. The absorber features a centrosymmetric square block array design, incorporating a PU conductive film as the surface resonant material. By fine-tuning the parameters of each component in the absorber's equivalent circuit and optimizing structural parameters, the absorber achieves an extended bandwidth from 3.92 to 15.25 GHz, with a relative absorption bandwidth of 118.21%. Impressively, in the lower frequency C-band, the absorber maintains an efficiency of over 95%. The absorber was fabricated using the "cut-transfer-paste patterning method." Testing results demonstrate that it is insensitive to incident angle and polarization and retains excellent absorption performance even when being bent.

1. INTRODUCTION

The advancement of technology has led to the widespread use of low-frequency radars in various fields, resulting in increased electromagnetic pollution [1]. This pollution has been linked to a higher risk of cancer, especially for those working or living near radar stations. The World Health Organization (WHO) has long recognized this issue as a significant health concern. Traditional electromagnetic protection equipment, developed through conventional methods, often struggles with high costs, complex manufacturing processes, and limited absorption bandwidths [2–4].

Since Landy et al. first proposed metamaterial absorbers in 2008 [5], absorbers have attracted considerable attention for their efficiency, thinness, and ease of fabrication. Recent research on wearable metamaterial absorbers has primarily focused on designs using thin-film organic substrates, showing promising results [6–9, 19]. However, the weight, poor flexibility, and lack of breathability associated with organic materials limit their effectiveness in wearable electromagnetic protection equipment.

Fabric-based metamaterial absorbers provide enhanced flexibility and breathability for wearable applications. However, the low dielectric constant of fabrics impacts the characteristic impedance of the dielectric layer, leading to reduced absorption rates at low frequencies [10]. Consequently, designing broadband metamaterial absorbers that achieve high absorption rates at low frequencies remains challenging, attracting considerable research interest.

Lee et al. used screen printing technology to apply silver conductive ink on fabric, creating a wearable metamaterial absorber with high absorption at 10.8 GHz [11]. Yang et al. utilized a computerized embroidery machine to embroider silver-coated nylon threads onto scuba knit fabric, achieving a 99% absorption rate at 2.39 GHz [12]. Similarly, Tak and Choi embroidered conductive metalized nylon fabric onto felt, creating a flexible absorber with two absorption peaks greater than 90% at 9 and 9.85 GHz; this absorber maintained high absorption rates even when being bent, though its relative absorption bandwidth was only 18.9% [13]. Sen et al. designed a dual-band absorber based on fabric, achieving absorption at 6.18 and 10.77 GHz, with a relative absorption bandwidth of 39.53% at high frequencies [14]. Yang et al. proposed a metamaterial absorber composed of a resistor film pattern, scuba knit fabric, and metalized fabric, achieving broadband absorption in the 8.9–15.2 GHz and 11.2–24.1 GHz ranges by adjusting the resistance of the resistor film [15]. Singh et al. used screen printing technology to print periodic patterns on plain and twill fabrics, designing absorbers with over 90% absorption in the 7.39–18 GHz range [16]. Celenk et al. designed a metamaterial absorber composed of conductive fabric and felt, achieving broadband absorption in the 13.1–31.13 GHz range [17]. Although significant progress has been made in extending the absorption bandwidth of fabric-based metamaterial absorbers, effective low-frequency absorption and bandwidth enhancement remain underexplored.

* Corresponding author: Yanjie Ju (746610878@qq.com).

Building on previous research, we propose a low-frequency, wearable broadband metamaterial absorber made from textiles. The design utilizes a soft, highly conductive PU film as the surface resonant material. The surface pattern, comprising two sets of square structures, extends the bandwidth through resonance peak superposition. This absorber is soft, breathable, cost-effective, and easy to fabricate, fully covering the C- and X-band frequencies. A physical sample of the broadband absorber was fabricated and experimentally validated in a microwave anechoic chamber, with results aligning well with the theoretical expectations.

2. STRUCTURAL DESIGN AND SIMULATION ANALYSIS

2.1. Structural Design

The proposed fabric-based broadband metamaterial absorber (FBBMA) consists of three main components: a frequency-selective surface, a dielectric layer, and a metallic ground plane. The dielectric layer, made of felt, has a dielectric constant (ε) of 1.9 and a loss tangent of 0.045. The frequency-selective surface comprises nine squares of three different sizes, utilizing a PU conductive film as the conductive material. In the simulation, this film is modeled as a sheet resistor with a square resistance (Rs) of 100 $\Omega/\square$. The structure and parameters of each component are detailed in Fig. 1.

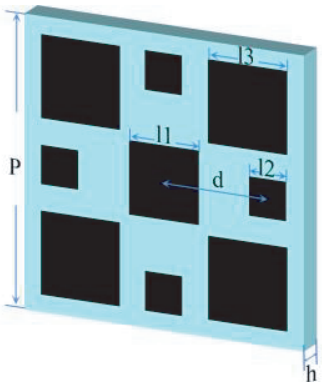

FIGURE 1. Unit model of the proposed FBBMA.

To thoroughly explore the electromagnetic wave absorption mechanism of the proposed FBBMA, an equivalent circuit model was constructed, as shown in Fig. 2. Efficient absorption by metamaterial absorber relies on the impedance matching mechanism, which was analyzed with the FBBMA's absorption performance. Impedance matching maximizes the entry of electromagnetic waves into the medium layer, thereby minimizing reflection and transmission. The input impedance (Z_{in}) of the FBBMA can be calculated as follows:

$$Z_{in}=\frac{Z_{sub}*Z_{FSS}}{Z_{sub}+Z_{FSS}} \tag{1}$$

The characteristic impedance of the felt medium is given by $Z_{sub}=\omega\mu_0/k_{sub}$, and its propagation constant is $k_{sub}=\omega\sqrt{\varepsilon_0\varepsilon_{sub}\mu_0}$. Here, ω is the angular frequency of the

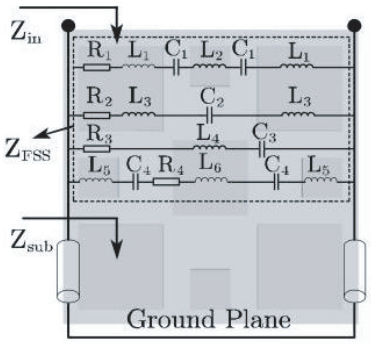

FIGURE 2. Equivalent circuit diagram.

electromagnetic wave, while ε_0 and μ_0 are the permittivity and permeability of free space, respectively. The dielectric constant of the felt medium is denoted as ε_{sub}, and the characteristic impedance of the frequency-selective surface is referred to as Z_{FSS}. Each of the four branches in the circuit can be simplified as an RLC series circuit. Therefore, the characteristic impedance of the frequency-selective surface can be calculated using the equivalent circuit model, as follows:

$$Z_{FSS}=\sum_{j=1}^{4}\frac{1}{Z_j} \tag{2}$$

In this context, $Z_{j\epsilon[1,4]}$ represents the equivalent impedance of the j-th branch formed by four RLC series circuits connected in parallel; Z_j can be calculated as follows:

$$Z_j=R_j+\frac{1}{j\omega C_j}+j\omega L_j \tag{3}$$

The reflection coefficient serves as a critical indicator of absorber performance. When electromagnetic waves strike the absorber's surface, the reflection coefficient Γ can be determined as follows:

$$\Gamma=\frac{Z_{in}-\eta_0}{Z_{in}+\eta_0} \tag{4}$$

Here, Z_{in} denotes the input impedance of FBBMA, and η_0 denote the wave impedance of free space, both normalized. Following this normalization, the reflection coefficient can be calculated as follows:

$$\Gamma=\frac{\overline{Z}_{in}-1}{\overline{Z}_{in}+1} \tag{5}$$

In the equation, $\overline{Z}_{in}=r+jx$ represents the normalized impedance of FBBMA. According to Equation (5), achieving a reflection coefficient Γ approaching zero requires the $\overline{Z}_{in}$ to approach unity. The $\overline{Z}_{in}$ can be calculated as follows:

$$\overline{Z}_{in}=\sqrt{\frac{(1+S_{11})^2-S_{21}^2}{(1-S_{11})^2-S_{21}^2}} \tag{6}$$

Efficient absorption is only achievable when the real part of $\overline{Z}_{in}$ approaches 1, and the imaginary part approaches 0. The reflection coefficient S_{11} directly determines these real and imaginary parts of the normalized impedance.

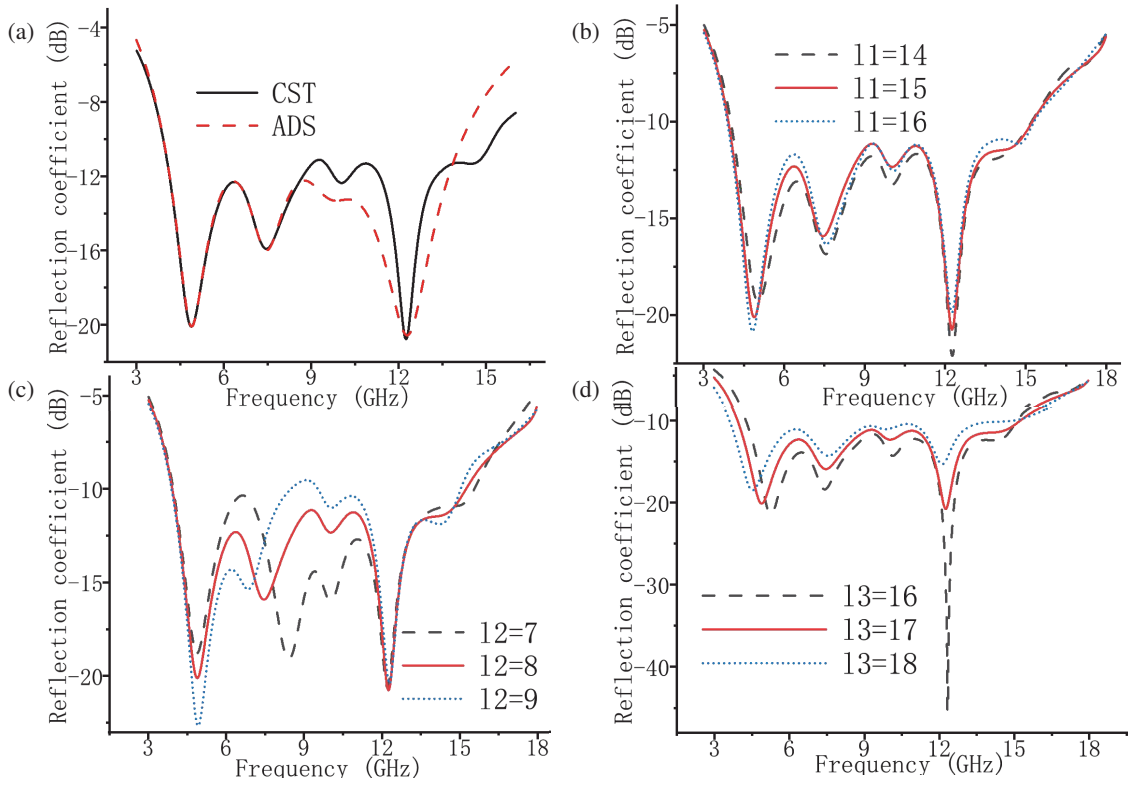

FIGURE 3. (a) Reflection coefficient graph obtained from equivalent circuit simulation using ADS. Changes in the reflection coefficient caused by structural variations in each unit: (b) $l1$, (c) $l2$, (d) $l3$.

TABLE 1. Equivalent circuit parameters.

R_1 (ohm)	R_2 (ohm)	R_3 (ohm)	R_4 (ohm)	C_1 (pF)	C_2 (pF)	C_3 (pF)
48.16	58.01	250.51	36.54	0.17731	0.370063	0.016092
C_4 (pF)	**L_1 (nH)**	**L_2 (nH)**	**L_3 (nH)**	**L_4 (nH)**	**L_5 (nH)**	**L_6 (nH)**
0.186014	1.9655	1.254	1.7576	16.685	0.5499	0.7127

2.2. Structural Optimization and Simulation

S_{11} is influenced directly by various parameters within the unit structure, which are derived using an equivalent circuit model in this study. Variations in the capacitance and inductance values within each branch cause shifts in resonance peaks, which are distributed evenly across the absorption band to optimize absorption. Additionally, resistance values are adjusted appropriately to enhance the amplitude of these resonance peaks. Detailed parameters of the equivalent circuit components are listed in Table 1, and simulation results are depicted in Fig. 3(a).

Based on the obtained component parameters, the structure parameters were optimized within a specific range. As depicted in Fig. 3(b), reducing $l1$ decreases the capacitance values of C3 and C4, causing a blue shift in the absorption band. As depicted in Fig. 3(c), increasing $l2$ increases the capacitance value of C1, causing both a red shift in the resonance peak and weakening of the superposition resonance effect with adjacent high-frequency resonance peaks. As depicted in Fig. 3(d), a decrease in $l3$ reduces the capacitance values of C1 and C2, leading to a blue shift in the resonance peak and a weakened absorption effect of FBBMA in the low-frequency range.

The final optimized structural parameters are $h = 5\,\text{mm}$, $l1 = 15\,\text{mm}$, $l2 = 8\,\text{mm}$, $l3 = 17\,\text{mm}$, $d = 22.5\,\text{mm}$, and $p = 60\,\text{mm}$. The reflection coefficient S_{11} was obtained through simulation, and the absorption rate $A(\omega)$ can be calculated as follows:

$$\begin{aligned} A(\omega) &= 1 - R(\omega) - T(\omega) \\ &= 1 - |S_{11}|^2 - |S_{21}|^2 \end{aligned} \tag{7}$$

The reflectance and transmittance are denoted as $R(\omega)$ and $T(\omega)$, respectively. It is generally assumed that $T(\omega) = S_{21} = 0$ because the metal grounding plate of the sample is much thicker than the skin depth of the electromagnetic wave. The curves of S_{11} and absorption rate $A(\omega)$ obtained are presented in Fig. 4. The proposed FBBMA achieves effective absorption rates exceeding 90% within the frequency range of 3.92 to 15.25 GHz. This absorption band spans the S, C, X, and Ku bands, resulting in a relative absorption bandwidth of 118%, demonstrating excellent broadband absorption capabilities.

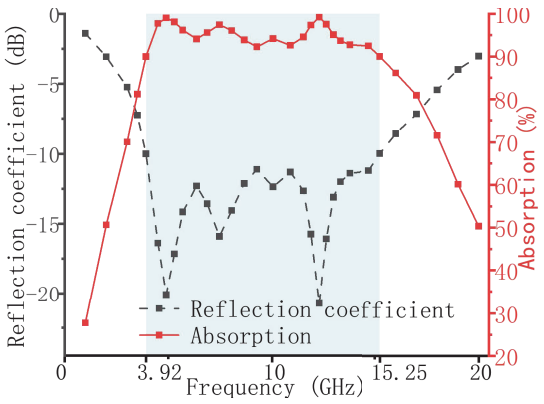

FIGURE 4. Reflection coefficient and absorption rate curves.

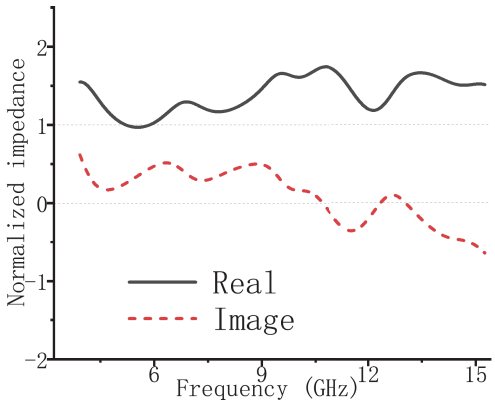

FIGURE 5. Curves of the real and imaginary parts of the normalized impedance.

2.3. Absorption Mechanism Analysis

Based on Equation (6), the normalized impedance curves of the real and imaginary parts are shown in Fig. 5. Within the absorption band, the real and imaginary parts approach 1 and 0, respectively, indicating impedance matching with the free-space impedance.

To broaden the absorption bandwidth, the technique of resonant peak superposition was employed. The FBBMA consists of two sets of structures, as depicted in Fig. 6. These structures generate resonant peaks around 4.895, 10.044, 12.25, and 7.46 GHz. These structures, when being combined, result in absorption peaks at these four resonant frequencies.

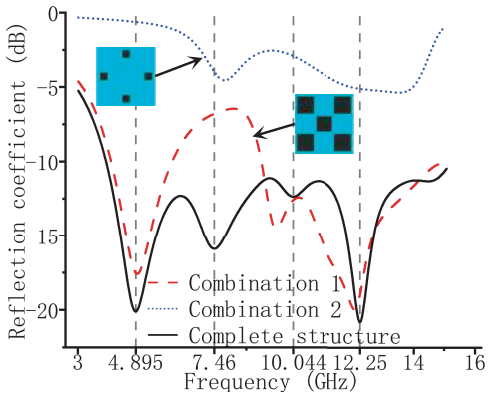

FIGURE 6. Two sets of structures and corresponding reflection coefficient curves.

Metamaterial absorbers efficiently absorb electromagnetic waves due to the excellent conductivity and high sheet resistance of the PU conductive film. When electromagnetic waves hit the absorber surface, significant resonant and Ohmic losses occur. In this study, we have focused on analyzing the current and electric field distributions at 4.9 GHz in the TE mode. As depicted in Fig. 7, the current predominantly flows along the left and right sides of the square structure with side lengths $l1$ and $l3$. This current alignment results in substantial Ohmic loss and induces inductive characteristics. Moreover, the high electric field intensity at the upper and lower edges of the square structure with side lengths $l1$ and $l2$ causes a significant charge accumulation, leading to strong resonant loss and capacitive characteristics. The combined inductive and capacitive effects excited by the electromagnetic waves induce a robust resonance at 4.9 GHz in the absorber.

2.4. Characterization of Absorbers

The reflection coefficient and absorption rate curves of the FBBMA under both TE and TM polarization waves are depicted in Fig. 8. It is evident that neither the reflection coefficient nor the absorption rate is influenced by the polarization mode of the incident wave, demonstrating that the designed FBBMA is polarization-insensitive.

Additionally, the effect of large-angle incidence on the absorption rate was investigated, as illustrated in Fig. 9. While increasing the incidence angle does affect the absorption rate, it remains above 90% across a broad frequency band for incidence angles up to 30°. Even at 45°, the absorption rate stays above 85%, confirming that the proposed FBBMA demonstrates angle insensitivity.

Given the operational demands of the sample in specialized environmental conditions, this study conducts a detailed simulation and analysis of the effects of temperature and humidity on the electromagnetic absorption performance of FBBMA. The selected PU conductive film and felt material demonstrate stable physical properties, with their electrical characteristics showing minimal sensitivity to temperature within the range tolerable by the human body. Although variations in environmental humidity can influence the conductivity of the felt material, this effect remains insignificant. Thus, it is more pertinent to assess the impact under extreme conditions, specifically when the FBBMA dielectric layer is fully saturated with rainwater of a certain conductivity. The corresponding effect on the reflection coefficient is thoroughly evaluated, with the results depicted in Fig. 10(a). Fig. 10(b) provides a more comprehensive and intuitive illustration of the variations in the reflection coefficient. These findings suggest that environmental humidity has a negligible influence on the electromagnetic absorption performance of the FBBMA, even under severe conditions.

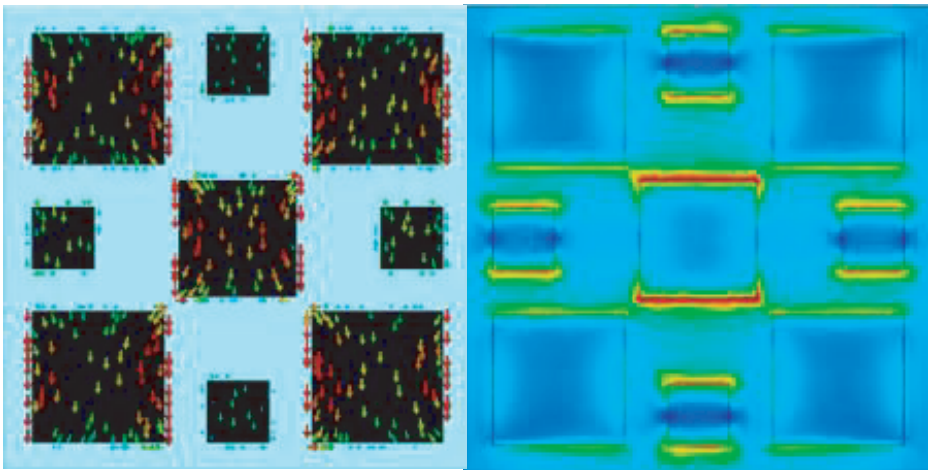

FIGURE 7. Current distribution and electric field distribution.

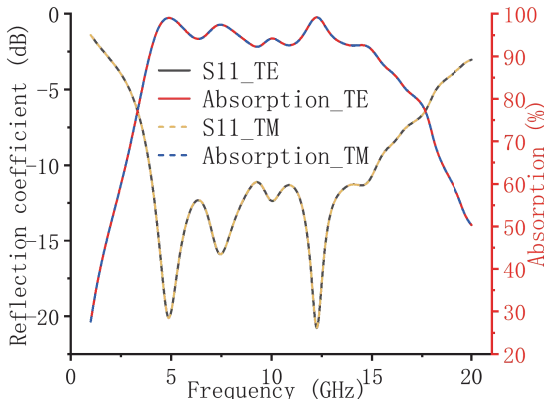

FIGURE 8. Polarization insensitivity characteristic curve.

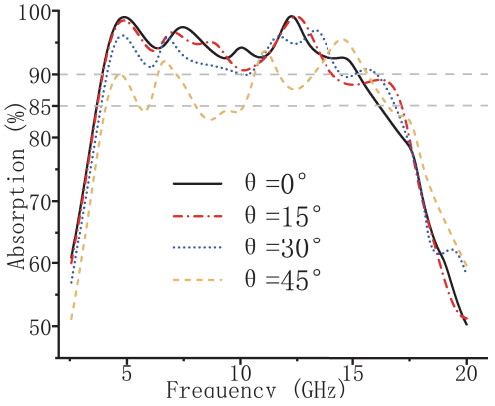

FIGURE 9. Incident angle insensitive characteristic curve.

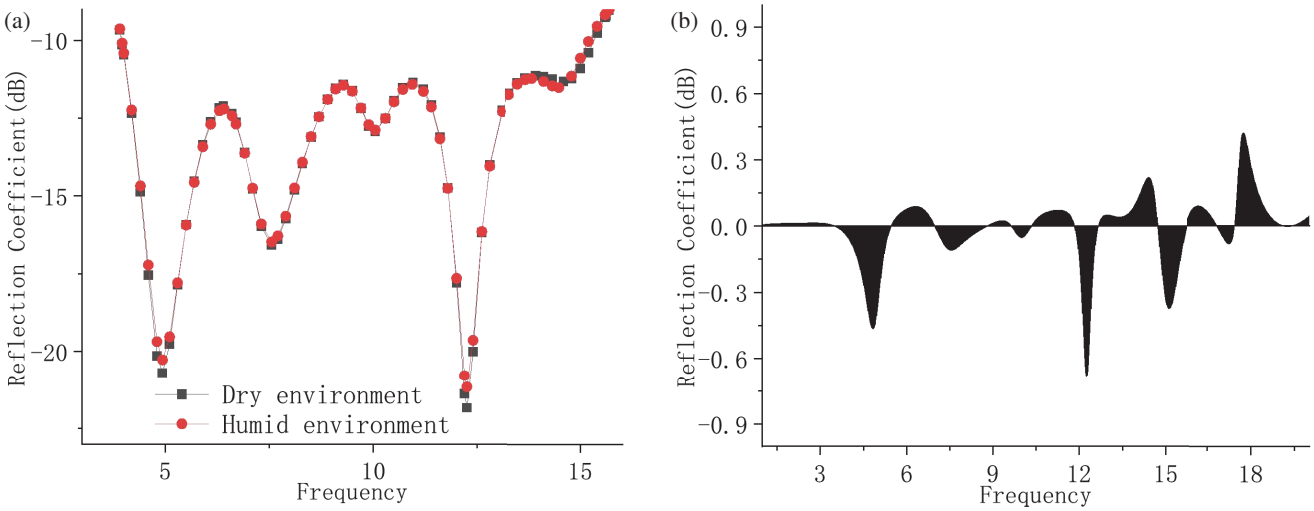

FIGURE 10. (a) Reflection coefficients of FBBMA under dry and wet conditions; (b) Difference in reflection coefficients between dry and wet conditions for FBBMA.

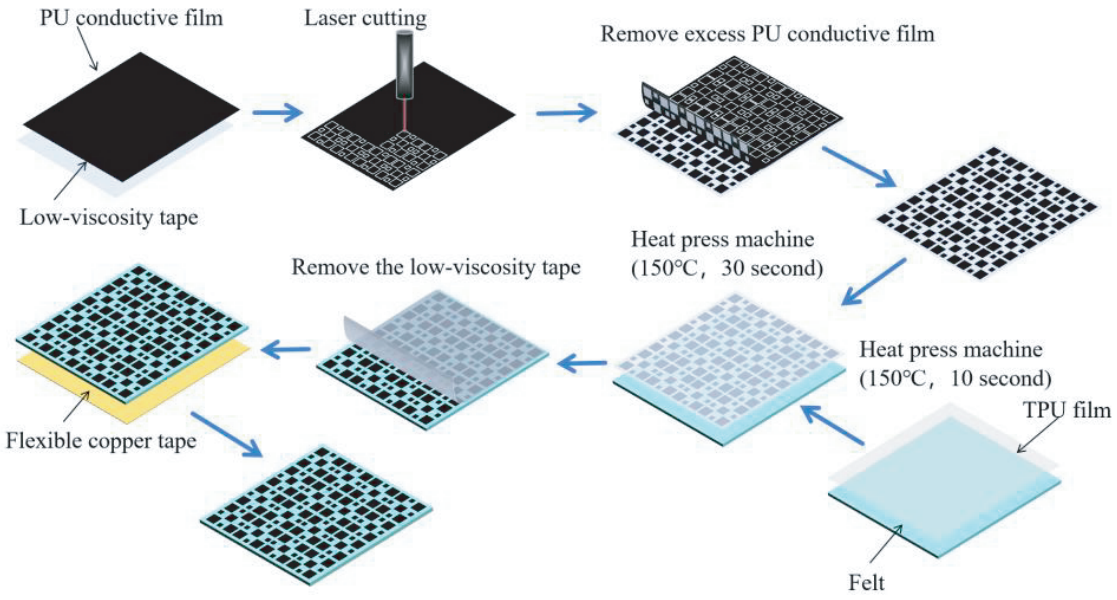

FIGURE 11. Flowchart of the sample preparation process.

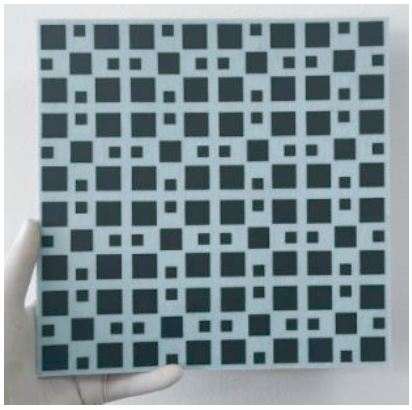

FIGURE 12. Fabricated sample.

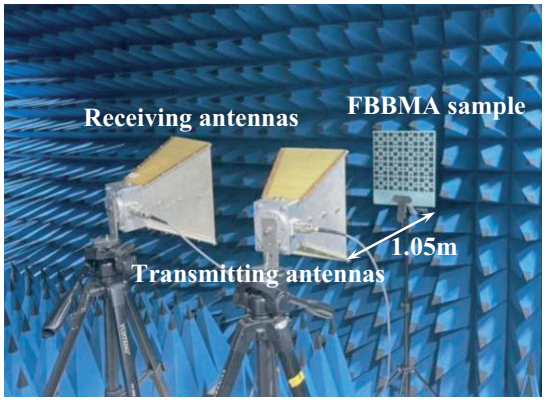

FIGURE 13. Samples with antennas in a darkroom.

3. SAMPLE PREPARATION AND EXPERIMENTAL TESTING

3.1. Preparation of Samples

In this study, samples consisting of 4×4 structural units measuring 260 mm $\times$ 260 mm were created using the "cut-paste-transfer pattern method," as illustrated in Fig. 11. Initially, a PU conductive film was secured onto low-viscosity tape to prevent positional shifts during the laser cutting. Precise control over laser power and cutting speed was maintained to prevent metal shrinkage due to high temperatures and ensure clean cuts. After cutting, excess material was carefully removed. Since the PU conductive film cannot directly adhere to the felt substrate, a heat-transfer TPU film was used as an adhesive medium. The TPU film was heat-pressed onto the felt substrate at 150°C for 10 s using a heat press machine. Subsequently, the patterned PU conductive film, along the TPU film, was placed over the felt substrate and heat-pressed at 150°C for 30 s. Following this, the low-viscosity transfer tape was removed. To ensure uniform heat distribution and prevent melting, and the PU conductive film and TPU film were covered with a layer of paper during the heat-pressing process.

A thin, flexible copper tape was selected as the metal grounding material and adhered to the back of the felt substrate using its adhesive properties. The final sample is depicted in Fig. 12.

3.2. Measured in a Darkroom

S_{11} parameter was measured using a network vector analyzer (KEYSIGHT N5247B) and two double-ridged horn antennas operating in the 2–18 GHz frequency range. The measurements were conducted in a microwave anechoic chamber using free-space test method. To ensure accurate measurements, the angle between the transmitting and receiving antennas was kept below 10°, and the distance d between the antenna and the sample

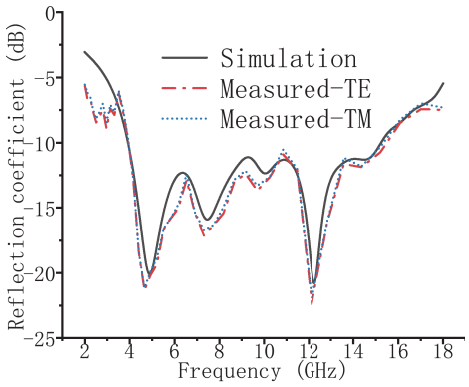

FIGURE 14. Reflection coefficient curve and polarization insensitivity characteristics of the sample.

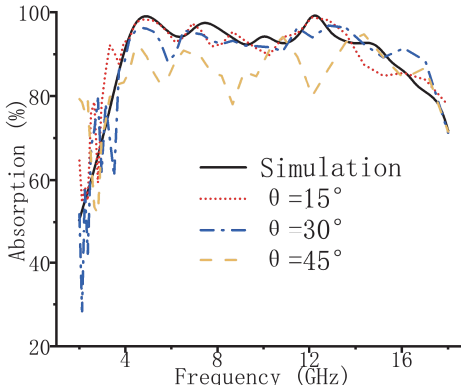

FIGURE 15. Test results showing incident angle insensitivity of the sample.

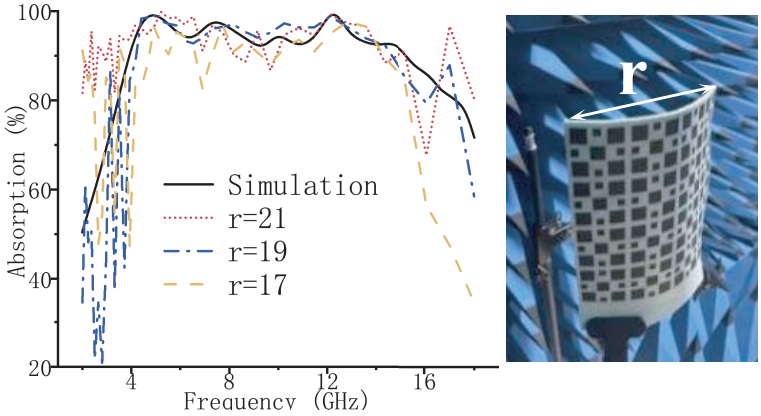

FIGURE 16. Curve showing absorption rate test result of bent sample.

TABLE 2. Previous related research.

Ref.	Absorption bands/GHz	Relative Bandwidth	Cost	Wearable	Breathability
[15]	$8.9 \sim 15.2/11.2 \sim 24.1$	52.28%/73.09%	low	Yes	Yes
[16]	$7.39 \sim 18$	83.58%	Med.	Yes	Yes
[18]	$6.3 \sim 14.2$	77.07%	High	No	No
[19]	$7.88 \sim 18.01$	78.25%	High	Yes	No
[17]	$13.1 \sim 31.13$	81.53%	Med.	Yes	Yes
This work	$3.92 \sim 15.25$	118.21%	low	Yes	Yes

adhered to the far-field condition specified in Equation (8):

$$d \geq \frac{2D^2}{\lambda} \tag{8}$$

where D represents the sample size, and λ denotes the wavelength. For this study, the distance between the sample and the antenna should be no less than 1.05 m. The setup of the sample and antenna within the microwave anechoic chamber is illustrated in Fig. 13.

Initially, the reflection coefficient and polarization-insensitive characteristics of the sample were measured and validated, with the results presented in Fig. 14. The reflection coefficient obtained via the free-space method closely aligns with the simulation results, confirming the sample's polarization insensitivity.

Following this, experiments were conducted to confirm the sample's insensitivity to the angle of incidence. As depicted in Fig. 15, the sample maintains an absorption rate of over 90% for incidence angles up to 30°. Even at an incidence angle of 45°, the absorption rate decreases but remains above 80%. These experimental findings closely correspond with the simulation results, thereby validating the designed FBBMA's insensitivity to the angle of incidence.

The flexibility of the sample was also assessed, as illustrated in Fig. 16. As the bending radius (r) decreases, the degree of bending increases. Absorption rates were measured and cal-

culated for samples with bending radii values of 17, 19, and 21 cm. While the absorption rate shows a slight decrease under bending conditions, it remains above 90%, with only minimal reduction in absorption bandwidth. This underscores that the proposed FBBMA maintains high absorption efficiency even when being subjected to bending.

To highlight the superiority of the designed metamaterial absorber, we compare it with previously obtained absorbers in terms of absorption bandwidth, relative bandwidth, and cost-effectiveness, as detailed in Table 2. The proposed FBBMA demonstrates efficient absorption at lower frequencies and boasts a larger relative bandwidth. Its excellent flexibility and breathability enhance its wearability. Moreover, the fabrication process utilizes inexpensive materials like felt and PU conductive film, employing laser cutting machines and heat presses, ensuring low cost and ease of manufacturing.

4. CONCLUSION

In this study, we present a flexible metamaterial absorber based on fabric, employing a PU conductive film as the surface resonant material. The absorption bandwidth is expanded using resonance peak superposition, achieving efficient absorption through the induced Ohmic and resonance losses. Simulation results demonstrate that the proposed FBBMA achieves over 90% broadband absorption within the 3.92–15.25 GHz range. This operational frequency range spans the S, C, X, and Ku bands, with a remarkable relative absorption bandwidth up to 118.21%.

Furthermore, the FBBMA sample was fabricated using the "cut-paste-transfer pattern method" and tested in a microwave anechoic chamber. The experimental results closely match the simulation, confirming consistent high-efficiency absorption of electromagnetic waves across a 45° incident angle range. The sample exhibited consistent absorption performance under both TE and TM polarization modes, showcasing its polarization-insensitive properties. Additionally, the flexibility of the proposed absorber sample was confirmed, suggesting that the sample retained its softness and excellent absorption performance even when being bent.

In summary, the proposed FBMA offers significant advantages including broad absorption bandwidth, suitability for low-frequency bands, flexibility, cost-effectiveness, and ease of fabrication. These qualities position it as an innovative solution for wearable electromagnetic protection equipment.

ACKNOWLEDGEMENT

This work was supported in part by the Natural Science Project of Liaoning Education Department under Grant ID LJKZ0485.

REFERENCES

[1] Amit, V., K. Vijay, and G. Shipra, "Bio-effects of 5th generation electromagnetic waves on organs of human beings," *Global Health Journal*, Vol. 7, No. 4, 206–211, 2023.

[2] Rathour, R., J. Krishnasamy, A. Das, and R. Alagirusamy, "Water vapor transmission and electromagnetic shielding characteristics of stainless steel/viscose blended yarn woven fabrics," *Journal of Industrial Textiles*, Vol. 53, No. 2, 152808372211492, 2023.

[3] Chen, T., F. Zhou, X. Cai, T. Liu, K. Qian, Z. Zhang, L. Duan, X. Dai, and K. Yu, "Flexible electromagnetic wave absorption material: Multiscale synergistic approach to achieve whole X-band absorption and thermal stealth property," *Carbon*, Vol. 210, 118048, 2023.

[4] Shakir, H., T. Zhao, K. Zubair, M. K. Sarwar, Z. Rehan, K. Fatima, and H. Aziz, "Fabrication and EMI (electromagnetic interference) shielding performance of polyester fabrics coated with polyaniline via in-situ polymerization," *Materials Today Communications*, Vol. 37, 106971, 2023.

[5] Landy, N. I., S. Sajuyigbe, J. J. Mock, D. R. Smith, and W. J. Padilla, "Perfect metamaterial absorber," *Physical Review Letters*, Vol. 100, No. 20, 207402, 2008.

[6] Alsulami, Q. A., S. Wageh, A. A. Al-Ghamdi, R. M. H. Bilal, and M. A. Saeed, "A tunable and wearable dual-band metamaterial absorber based on polyethylene terephthalate (PET) substrate for sensing applications," *Polymers*, Vol. 14, No. 21, 4503, 2022.

[7] Aqilafif, N., H. T. Yudistira, and F. Qalbina, "Design of tripartite square ring metamaterial absorber using polyvinyl chloride as a flexible substrate at S-band and C-band spectrums," *Journal of Materials Science: Materials in Electronics*, Vol. 34, No. 3, 199, 2023.

[8] Jing, H., Y. Wei, J. Kang, C. Song, H. Deng, J. Duan, Z. Qu, J. Wang, and B. Zhang, "An optically transparent flexible metasurface absorber with broadband radar absorption and low infrared emissivity," *Journal of Physics D: Applied Physics*, Vol. 56, No. 11, 115103, 2023.

[9] Rani, N., A. K. Bohre, and A. Bhattacharya, "A conformal ultra-thin and ultra-wideband metamaterial-based absorber dedicated for applications in C and X bands," *SN Computer Science*, Vol. 4, No. 5, 490, 2023.

[10] Costa, F., S. Genovesi, A. Monorchio, and G. Manara, "A circuit-based model for the interpretation of perfect metamaterial absorbers," *IEEE Transactions on Antennas and Propagation*, Vol. 61, No. 3, 1201–1209, 2012.

[11] Lee, D., H. K. Kim, and S. Lim, "Textile metamaterial absorber using screen printed chanel logo," *Microwave and Optical Technology Letters*, Vol. 59, No. 6, 1424–1427, 2017.

[12] Yang, Y., J. Wang, C. Song, R. Pei, J. M. Purushothama, and Y. Zhang, "Electromagnetic shielding using flexible embroidery metamaterial absorbers: Design, analysis and experiments," *Materials & Design*, Vol. 222, 111079, 2022.

[13] Tak, J. and J. Choi, "A wearable metamaterial microwave absorber," *IEEE Antennas and Wireless Propagation Letters*, Vol. 16, 784–787, 2016.

[14] Sen, G., M. Kumar, S. N. Islam, and S. Das, "A dual band wearable metamaterial absorber with reduced cross-polarized reflection," in *2018 3rd International Conference on Microwave and Photonics (ICMAP)*, 1–2, Dhanbad, India, Feb. 2018.

[15] Yang, Y., C. Song, R. Pei, J. Wang, Z. Liu, Y. Zhang, and J. Shen, "Design, characterization and fabrication of a flexible broadband metamaterial absorber based on textile," *Additive Manufacturing*, Vol. 69, 103537, 2023.

[16] Singh, G., H. Sheokand, K. Chaudhary, K. V. Srivastava, J. Ramkumar, and S. A. Ramakrishna, "Fabrication of a non-wettable wearable textile-based metamaterial microwave absorber," *Journal of Physics D: Applied Physics*, Vol. 52, No. 38, 385304, 2019.

[17] Celenk, E., C. Lynch, and M. M. Tentzeris, "An ultra-wideband all-textile metamaterial absorber for Ku-, K-, and Ka-band applications," *IEEE Antennas and Wireless Propagation Letters*, Vol. 23, No. 6, 1789–1793, 2024.

[18] Malik, S., M. Saikia, A. Sharma, G. Singh, G. Saptarshi, P. K. Mishra, and K. V. Srivastava, "Design and analysis of polarization-insensitive broadband microwave absorber for perfect absorption," *Progress In Electromagnetics Research M*, Vol. 104, 213–222, 2021.

[19] Long, L. V., N. S. Khiem, B. S. Tung, N. T. Tung, T. T. Giang, P. T. Son, B. X. Khuyen, V. D. Lam, L. Chen, H. Zheng, and Y. Lee, "Flexible broadband metamaterial perfect absorber based on graphene-conductive inks," in *Photonics*, Vol. 8, No. 10, 440, 2021.